Available online at www.sciencedirect.com

SciVerse ScienceDirect

Ceramics International 39 (2013) 3533–3538

CERAMICS INTERNATIONAL

www.elsevier.com/locate/ceramint

Facile one-step solid-state reaction route to synthesize ordered mesoporous β-Zn_2SiO_4–SiO_2 nanocomposites

Qingshan Lu[a,*], Guohong Yun[a,b]

[a]*Inner Mongolia University, College of Physical Science and Technology, 235 West Daxue Street, Hohhot 010021, China*
[b]*College of Physics and Electronic Information, Inner Mongolia Normal University, Hohhot 010022, China*

Received 21 July 2012; received in revised form 24 September 2012; accepted 8 October 2012
Available online 16 October 2012

Abstract

Ordered crystalline mesoporous β-Zn_2SiO_4–SiO_2 nanocomposites were prepared by one-step solid-state reaction using mesoporous silica as both template and silica source. Zinc oxide formed by decomposition of zinc nitrate reacts with mesoporous silica and the β-Zn_2SiO_4 forms and disperses inside the silica walls. The obtained β-Zn_2SiO_4–SiO_2 nanocomposites possess hexagonal mesostructure with the β-Zn_2SiO_4 weight percentage below 40%. The β-Zn_2SiO_4 nanocrystals are surrounded by the non-crystalline silica of mesoporous walls. The non-crystalline silica acting as a binder to stick β-Zn_2SiO_4 nanocrystals plays a role in restraining the phase transformation from β-Zn_2SiO_4 to α-Zn_2SiO_4 and increasing the thermal stability of mesoporous β-Zn_2SiO_4. The crystalline mesoporous β-Zn_2SiO_4 may be a potential candidate for application as absorbents, for separation and as phosphors.

Keywords: Mesoporous silica; Solid-state reaction; Zinc silicate; Mesostructure

1. Introduction

Since the first discovery of mesoporous M41S in 1992 [1], mesoporous materials have attracted considerable attention for their unique mesostructure, morphology, as well as composition. These result in their promising properties and great potential applications as catalysts, absorbents, gas sensors, solar cells, batteries, and electronics [2–6]. Up to now, mesoporous silica with a variety of mesostructures has been successfully fabricated [7]. The main shortcomings of the fabricated mesoporous silica are non-crystalline walls and single composition, which greatly limit their practical applications. Non-silica mesoporous materials such as transition metal oxides, multimetal oxides, phosphates, etc. have wide range of applications owing to their diverse electronic structures and textural compositions. A survey of existing literatures has shown that non-silica mesoporous materials are commonly prepared by the surfactant-assisted approach and nanocasting method [5,6,8]. Nevertheless, the study indicates that it is still a challenge to obtain ordered non-silica crystalline mesostructures. Taking the surfactant-assisted approach as an example, ordered mesostructures are formed by the co-assembly of surfactant and inorganic species [1,8]. At present, there exist two difficulties. Firstly, the hydrolysis and condensation reactions of non-silica precursors are difficult to be controlled and it is not easy to get proper inorganic oligomers for the self-assembly. Secondly, the mesostructures are obtained by removing the surfactant. During the calcination, the crystallization, grain growth, and phase transformation of mesoporous walls take place, which will lead to the loss of mesostructures [9]. The nanocasting method was developed to prepare non-silica mesoporous materials [6]. However, the reproducibility in obtaining high-quality crystalline mesoporous is bad [10]. The final products possess dispersed nanoparticles or nanowires instead of mesostructures. Additionally, this method involves a complicated process and has low yield.

An efficient method to resolve the problem mentioned above is to add amorphous components, such as silica, phosphoxides, and carbon, into the mesoporous walls [8,11]. The amorphous component which acts as a binder to stick non-silica nanocrystals in the walls is responsible for the stability of ordered mesostructures. Zhao et al. prepared mesoporous TiO_2–SiO_2 nanocomposites based

*Corresponding author. Tel.: +86 471 4993141.
E-mail address: luqs@imu.edu.cn (Q. Lu).

0272-8842/$ - see front matter © 2012 Elsevier Ltd and Techna Group S.r.l. All rights reserved.
http://dx.doi.org/10.1016/j.ceramint.2012.10.177

on sol–gel and evaporation-induced self-assembly technology [11]. The sample shows ordered two-dimensional mesostructure, uniform pore size, large specific surface areas, and high thermal stability. However, the synthesis condition such as hydrolysis–condensation reaction, the relative humidity, evaporation temperature, and calcination must be precisely controlled. Therefore, it is very important to explore a new facile strategy for preparing non-silica mesoporous materials with ordered mesostructure and high thermal stability.

Silicates are useful in many applications of technological fields. For example, silicates doped with rare-earth ions are efficient phosphors due to their high visible-light transparency, excellent luminescence efficiency, and chemical stability [12]. Besides, silicates with unique structures show great potential for ion exchange and absorption [13,14]. Recently, silicates have been reported as new cathode materials for rechargeable magnesium batteries [15]. No matter used as absorbents or cathode materials, the morphology, specific surface area, and pore size of silicates would play important roles in the properties.

In this work, we have demonstrated firstly a direct and facile approach to synthesize ordered crystalline mesoporous β-Zn_2SiO_4–SiO_2 nanocomposites by one-step solid-state reaction using mesoporous silica as both template and silica source. In the meantime, we have studied the microstructure and mesostructure of the obtained sample, and proposed a mechanism to explain the mesostructure generation process.

2. Experimental section

Parent mesoporous silica was synthesized according to the reported process [6]. The procedure of preparing mesoporous β-Zn_2SiO_4–SiO_2 nanocomposites is as follows. A solution was prepared by dissolving zinc nitrate hexahydrate in distilled water–ethanol solution. Then, the mesoporous silica was added to the above zinc nitrate solution. The resulting solution was stirred for 12 h in air at room temperature until all the solvent was completely evaporated for obtaining a dry powder. The dried powder was calcined at 800 °C for 4 h at a heating rate of 1 °C/min. The mesoporous β-Zn_2SiO_4–SiO_2 nanocomposites with different β-Zn_2SiO_4 loadings are referred to as x wt% β-Zn_2SiO_4–SiO_2, where x represents the weight percentage of β-Zn_2SiO_4 in the β-Zn_2SiO_4–SiO_2 nanocomposites.

The crystal structure and mesostructure of the samples were investigated by X-ray diffraction (XRD) on a Rigaku D/max-2400 X-ray diffractometer with Cu K_α radiation (40 kV, 60 mA) in the 2θ range of 10–80°. The measurement was performed at a scan rate of 5°/min with the step size of 0.02°. The microstructures of the samples were observed by a JEM 2010 high resolution transmission electron microscope operated with a voltage of 200 kV. The content of the element was analyzed using IRIS Advantage inductively coupled plasma atomic emission spectrometry (ICP-AES). The chemical interactions and bonding structures were analyzed by Fourier transform infrared spectra (FTIR) on a Nicolet Nexus 670 spectrometer. Nitrogen adsorption–desorption isotherms were measured using a Micromeritics ASAP2020 specific surface area analyzer.

3. Results and discussion

The low-angle XRD patterns of the β-Zn_2SiO_4–SiO_2 nanocomposites with different β-Zn_2SiO_4 weight percentages calcined at 800 °C for 4 h are shown in Fig. 1. All the XRD patterns show a sharp diffraction peak and two weak peaks. Three peaks can be indexed as (100), (110), and (200) diffractions of a two-dimensional hexagonal mesostructure [1,2]. This indicates that the β-Zn_2SiO_4–SiO_2 nanocomposites keep highly ordered mesostructure. The main diffraction peaks of the 10 wt%, 30 wt%, and 40 wt% β-Zn_2SiO_4–SiO_2 nanocomposites locate at $2\theta = 0.95°$, 1.00°, 1.03°, respectively. It is obvious that the peaks shift to large angle with increasing β-Zn_2SiO_4 weight percentage. This could be owing to the contraction of mesoporous walls resulted by the formation of β-Zn_2SiO_4 due to the solid-state reaction between zinc oxide and mesoporous silica during calcination. In addition, the intensity of two weak diffraction peaks of β-Zn_2SiO_4–SiO_2 nanocomposites becomes weak, suggesting that the mesostructure is a little degraded with increasing β-Zn_2SiO_4 loading.

Fig. 2 shows the high-angle XRD patterns of the β-Zn_2SiO_4–SiO_2 nanocomposites with different β-Zn_2SiO_4 weight percentages calcined at 800 °C for 4 h. All the samples exhibit the diffraction peaks overlapped on a broad diffraction halo. The diffraction halo is attributed to the non-crystalline silica because of the excess silica remaining in the final product. The diffraction peaks of all samples can be indexed as diffractions of β-Zn_2SiO_4 (β-phase) [16]. The diffraction peaks are broad due to the small crystallite size.

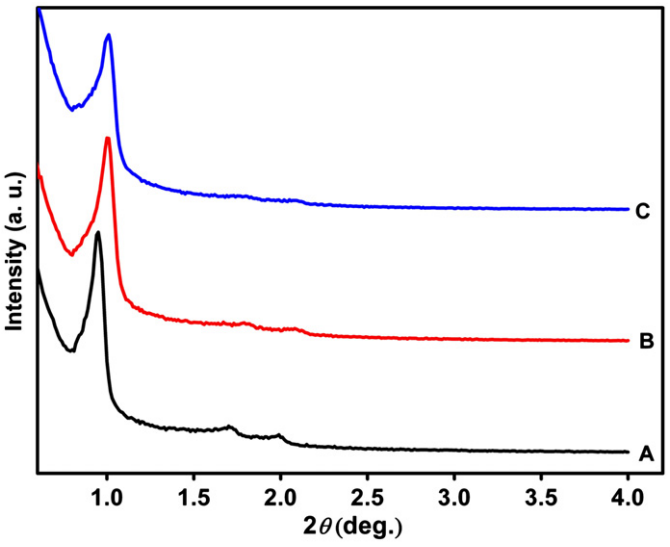

Fig. 1. Low-angle X-ray diffraction patterns of the β-Zn_2SiO_4–SiO_2 nanocomposites with β-Zn_2SiO_4 weight percentages of 10 wt% (A), 30 wt% (B), and 40 wt% (C) calcined at 800 °C for 4 h.

The XRD results indicate that crystalline β-Zn_2SiO_4 can be obtained by a solid-state reaction between ZnO (formed by decomposition of zinc nitrate) and mesoporous silica at a low calcination temperature of 800 °C. This reaction temperature is much lower than that of conventional solid-state reaction using dense silica powder as silica source [17]. Similar results are also obtained in our previous work [18]. The low reaction temperature is owing to the unique structure of mesoporous silica with large specific surface areas and porous structure which can greatly increase the reaction interfaces and decrease the diffusion distance among the reactants [19].

As is well known, β-Zn_2SiO_4 is a meta-stable phase and is quite stable at room temperature and it transforms to α-Zn_2SiO_4 (α-phase) at high temperature. In this study, β-Zn_2SiO_4 does not transform to α-Zn_2SiO_4 at 800 °C. Herein the mesoporous silica is abundant in the solid-state reaction. The ZnO reacts with silica walls and the formed β-Zn_2SiO_4 nanocrystals are embedded in the walls of mesoporous silica. The β-Zn_2SiO_4 could be considered to be surrounded by non-crystalline silica which acts as a binder to stick β-Zn_2SiO_4 nanocrystals. This is the same as the case of adding amorphous components, such as silica, phosphoxides, and carbon, into the non-silica mesoporous walls [8,11]. Therefore the non-crystalline silica not only suppresses the phase transformation from β-Zn_2SiO_4 to α-Zn_2SiO_4, but also increases the thermal stability of β-Zn_2SiO_4. This is similar to the reported results that the silica of mesoporous silica/titania nanocomposites could restrain the phase transformation from anatase to rutile TiO_2 [11].

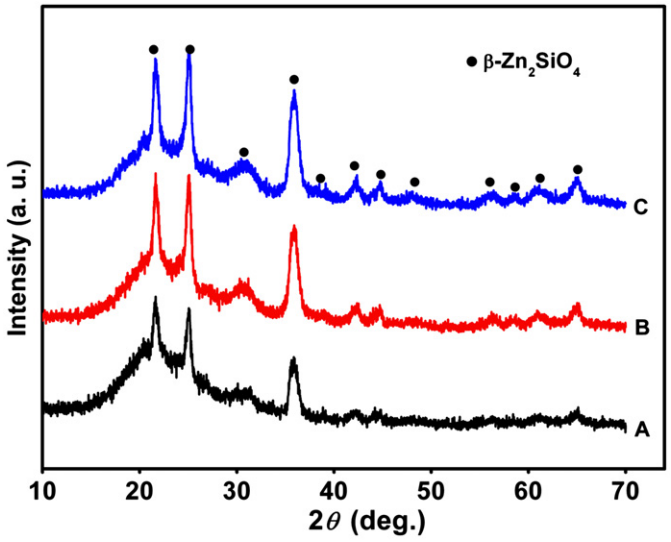

Fig. 2. High-angle X-ray diffraction patterns of the β-Zn_2SiO_4–SiO_2 nanocomposites with β-Zn_2SiO_4 weight percentages of 10 wt% (A), 30 wt% (B), and 40 wt% (C) calcined at 800 °C for 4 h.

Fig. 3 shows the TEM micrographs of 30 wt% β-Zn_2SiO_4–SiO_2 nanocomposites calcined at 800 °C for 4 h. Viewed along the electron beam perpendicular to channels, the parallel straight channels in Fig. 3a can be observed. While the electron beam is parallel to the channels, as shown in Fig. 3b, the sample shows the highly ordered honeycomb-like pore array structure. The TEM observation indicates that the 30 wt% β-Zn_2SiO_4–SiO_2 nanocomposites keep a two-dimensional hexagonal mesoporous structure same as that of parent mesoporous silica [10]. This is in good agreement with the low-angle XRD result. The small β-Zn_2SiO_4 nanocrystals could not be observed through TEM investigations, possibly due to the weak image contrast between silica walls and small β-Zn_2SiO_4 nanocrystals, as the case of metal oxides encapsulated inside mesoporous materials. The EDS analysis was carried out on the 30 wt% β-Zn_2SiO_4–SiO_2 nanocomposites with the EDS attachment on the TEM. As shown in Fig. 4, the C and Cu elements come from the supporting carbon film and the copper grid, respectively. The strong zinc signals can be clearly detected, confirming the presence of Zn element from β-Zn_2SiO_4. The Zn/Si molar ratio calculated from the EDS spectrum in Fig. 4 is about 0.18. Based on the Zn/Si molar ratio of 0.18, the weight percentage of β-Zn_2SiO_4 in the β-Zn_2SiO_4–SiO_2 nanocomposites is about 27% which is close to that obtained from reactant stoichiometry. In order to determine the weight

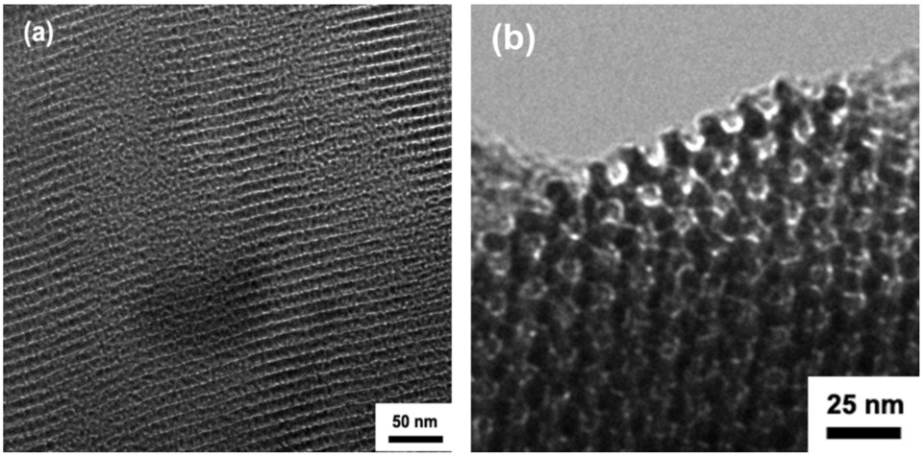

Fig. 3. Transmission electron microscope micrographs of the 30 wt% β-Zn_2SiO_4–SiO_2 nanocomposites calcined at 800 °C for 4 h: perpendicular to the channels (a) and parallel to the channels (b).

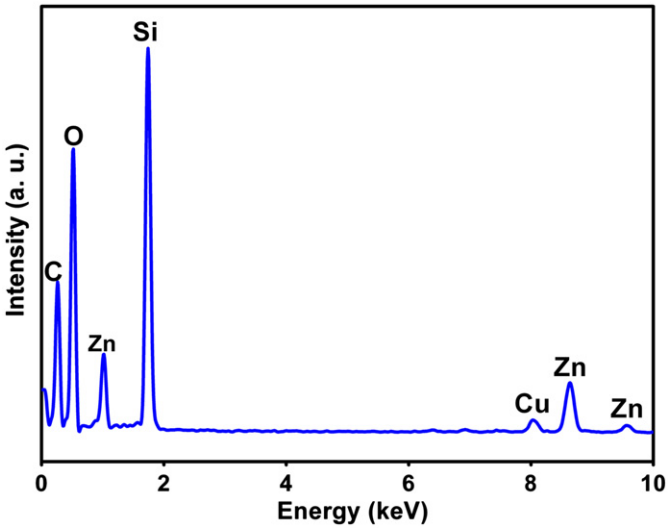

Fig. 4. Energy dispersive spectra of the 30 wt% β-Zn_2SiO_4–SiO_2 nanocomposites calcined at 800 °C for 4 h.

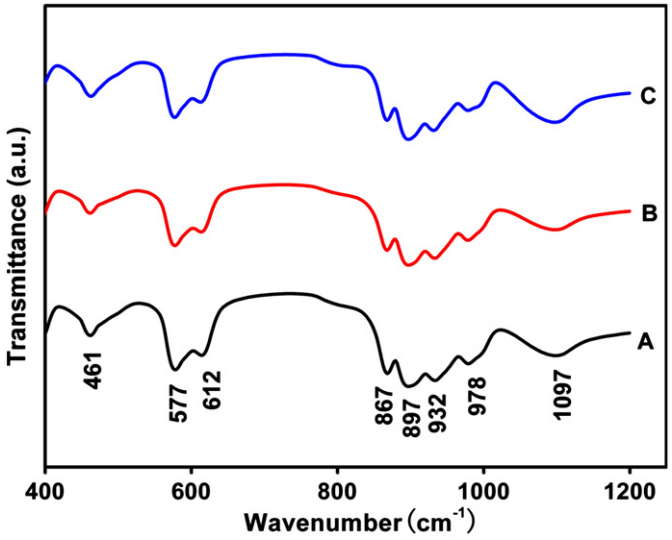

Fig. 5. Fourier transform infrared spectra of the β-Zn_2SiO_4–SiO_2 nanocomposites with β-Zn_2SiO_4 weight percentages of 10 wt% (A), 30 wt% (B), and 40 wt% (C) calcined at 800 °C for 4 h.

percentage of the β-Zn_2SiO_4 in β-Zn_2SiO_4–SiO_2 nanocomposites, the inductively coupled plasma atomic emission spectrometry was measured. The weight percentages of the element Zn and Si are 31.7% and 68.3%, respectively. The weight percentage of the β-Zn_2SiO_4 in β-Zn_2SiO_4–SiO_2 nanocomposites is calculated to be about 28% which is close to the 30% obtained from the initial reactant weight percentage.

To study the chemical interactions and bonding structures, Fig. 5 shows the FTIR spectra of the β-Zn_2SiO_4–SiO_2 nanocomposites with different β-Zn_2SiO_4 weight percentages calcined at 800 °C for 4 h. The main absorption bands of three samples are located in the frequency region between 400 and 1200 cm^{-1} [20]. The bands at around 867 and 461 cm^{-1} are originated from the symmetric stretching and the asymmetric deforming vibrations of the SiO_4 groups, and the bands at around 897, 932 and 978 cm^{-1} are related to the asymmetric stretching vibrations of the SiO_4 groups. The bands at around 577 and 612 cm^{-1} can be attributed to the symmetric stretching and asymmetric stretching vibrations of the ZnO_4 groups, respectively. The band at around 1097 cm^{-1} is assigned to the stretching vibration of Si–O–Si due to the excess silica. The FTIR spectra analysis indicates the presence of zinc silicate. This is well consistent with the XRD results.

The nitrogen adsorption–desorption isotherms of the 40 wt% β-Zn_2SiO_4–SiO_2 nanocomposites calcined at 800 °C for 4 h is shown in Fig. 6. The sample shows the type IV isotherms with H1-type hysteresis loop, typical for mesoporous material with a two-dimensional hexagonal structure [1,11], which is coincident with the results obtained from the low-angle XRD and TEM analysis. In comparison to parent mesoporous silica, the inflection point of the capillary condensation step for the 40 wt% β-Zn_2SiO_4–SiO_2 nanocomposites shifts to low relative pressure, indicating the reduction of the mesopore size. This result is coincident with the contraction of mesoporous walls caused by a solid-state reaction and calcination. The BET surface

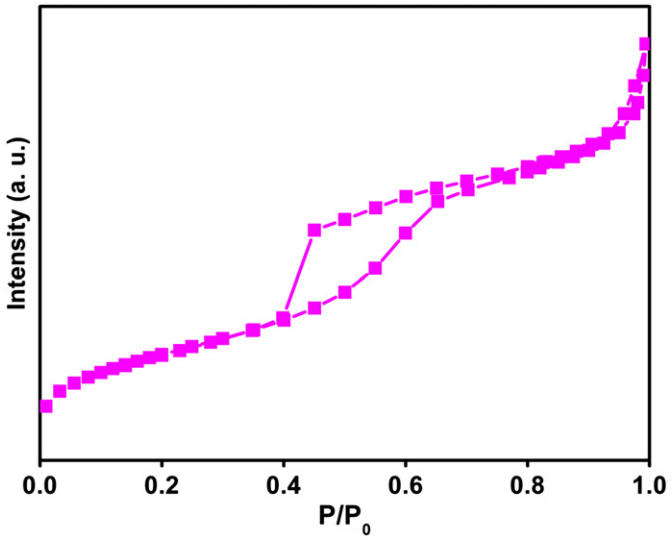

Fig. 6. N_2 adsorption–desorption isotherms of the 40 wt% β-Zn_2SiO_4–SiO_2 nanocomposites calcined at 800 °C for 4 h.

area of the sample is 326 m^2/g, which is a relative high specific surface area for non-silica mesoporous material. Crystalline mesoporous β-Zn_2SiO_4–SiO_2 nanocomposites with large specific surface areas are obtained firstly in this study. This approach is simple, low-costing, and easily reproducible and it may also be applied to prepare other crystalline mesoporous silicate materials.

A formation process of crystalline mesoporous β-Zn_2SiO_4–SiO_2 nanocomposites is proposed in Fig. 7. During the impregnation process, zinc nitrate solution is introduced into the nanoscale pores of mesoporous silica due to capillary forces. After low temperature calcination, zinc oxide formed by pyrolyzing zinc nitrate disperses on the inner surface of mesoporous silica. With further increasing calcination temperature, the zinc oxide reacts with mesoporous silica and the

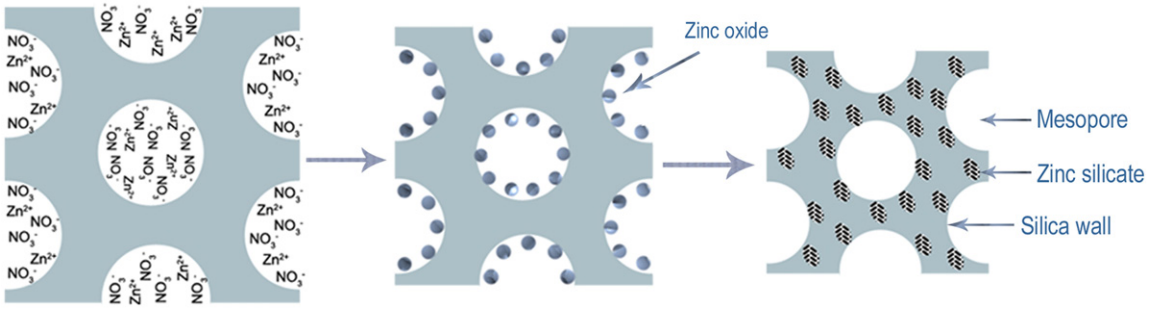

Fig. 7. A schematic diagram showing the formation of ordered crystalline mesoporous β-Zn_2SiO_4–SiO_2 nanocomposites.

crystalline β-Zn_2SiO_4 forms and grows along the silica walls at the cost of consumption of silica. As a result, after the zinc oxide is consumed, the formed β-Zn_2SiO_4 nanocrystals are embedded in the walls of mesoporous silica because of the excess of silica in the solid-state reaction. The β-Zn_2SiO_4 could be considered to be surrounded by non-crystalline silica as a binder to stick β-Zn_2SiO_4 nanocrystals, which makes sure that β-Zn_2SiO_4 does not transform into α-Zn_2SiO_4 at high temperature. Finally, the crystalline mesoporous β-Zn_2SiO_4–SiO_2 nanocomposites are formed. Based on these results, our approach is expected to be extended to prepare other crystalline mesoporous silicates.

4. Conclusions

A facile one-step solid-state reaction to prepare highly ordered mesoporous β-Zn_2SiO_4–SiO_2 nanocomposites is firstly demonstrated using mesoporous silica as both template and silica source. The zinc oxide formed inside the pores of mesoporous silica reacts with silica at 800 °C, and the crystalline β-Zn_2SiO_4 forms and grows along the silica walls. The obtained β-Zn_2SiO_4 nanocrystals are embedded in the non-crystalline silica of mesoporous silica which plays a role in increasing the thermal stability of β-Zn_2SiO_4 at high temperature. The β-Zn_2SiO_4–SiO_2 nanocomposites show highly ordered hexagonal mesostructure with the β-Zn_2SiO_4 weight percentage below 40%. The crystalline β-Zn_2SiO_4 with mesostructure has great potential to be applied as absorbents, filters, and phosphors.

Acknowledgments

This work was supported by the National Natural Science Foundation of China under Grant no. 51202103, the China Postdoctoral Science Foundation under Grant no. 2012M510789, the Natural Science Foundation of Inner Mongolia Autonomous Region under Grant no. 2011BS0804, the Program of Higher-level Talents of Inner Mongolia University under Grant no. Z20100123, and the Specialized Research Foundation for Postdoctoral Program of Inner Mongolia University under Grant no. 115303.

References

[1] C.T. Kresge, M.E. Leonowicz, W.J. Roth, J.C. Vartuli, J.S. Beck, Ordered mesoporous molecular sieves synthesized by a liquid-crystal template mechanism, Nature 359 (1992) 710–712.
[2] T. Yamada, H.S. Zhou, H. Uchida, M. Tomita, Y. Ueno, T. Ichino, I. Honma, K. Asai, T. Katsube, Surface photovoltage NO gas sensor with properties dependent on the structure of the self-ordered mesoporous silicate film, Advanced Materials 14 (2002) 812–815.
[3] I.I. Slowing, B.G. Trewyn, S. Giri, V.S.Y. Lin, Mesoporous silica nanoparticles for drug delivery and biosensing applications, Advanced Functional Materials 17 (2007) 1225–1236.
[4] X.Y. Hao, Y.Q. Zhang, J.W. Wang, W. Zhou, C. Zhang, S. Liu, A novel approach to prepare MCM-41 supported CuO catalyst with high metal loading and dispersion, Microporous and Mesoporous Materials 88 (2006) 38–47.
[5] J.H. Pan, W.I. Lee, Preparation of highly ordered cubic mesoporous WO_3/TiO_2 films and their photocatalytic properties, Chemistry of Materials 18 (2006) 847–853.
[6] W. Yue, W. Zhou, Synthesis of porous single crystals of metal oxides via a solid–liquid route, Chemistry of Materials 19 (2007) 2359–2363.
[7] J.Y. Ying, C.P. Mehnert, M.S. Wong, Synthesis and applications of supramolecular-templated mesoporous materials, Angewandte Chemie International Edition 38 (1999) 56–77.
[8] H. Zhou, D. Li, M. Hibino, I. Honma, A self-ordered, crystalline-glass, mesoporous nanocomposite for use as a lithium-based storage device with both high power and high energy densities, Angewandte Chemie International Edition 44 (2005) 797–802.
[9] B.L. Kirsch, E.K. Richman, A.E. Riley, S.H. Tolbert, In-situ X-ray diffraction study of the crystallization kinetics of mesoporous titania films, The Journal of Physical Chemistry B 108 (2004) 12698–12706.
[10] X. Sun, Y. Shi, P. Zhang, C. Zheng, X. Zheng, F. Zhang, Y. Zhang, N. Guan, D. Zhao, G.D. Stucky, Container effect in nanocasting synthesis of mesoporous metal oxides, Journal of the American Chemical Society 133 (2011) 14542–14545.
[11] W. Dong, Y. Sun, C.W. Lee, W. Hua, X. Lu, Y. Shi, S. Zhang, J. Chen, D. Zhao, Controllable and repeatable synthesis of thermally stable anatase nanocrystal–silica composites with highly ordered hexagonal mesostructures, Journal of the American Chemical Society 129 (2007) 13894–13904.
[12] L. Xiong, J. Shi, J. Gu, W. Shen, X. Dong, H. Chen, L. Zhang, J. Gao, M. Ruan, Directed growth of well-aligned zinc silicate nanowires along the channels of surfactant-assembled mesoporous silica, Small 1 (2005) 1044–1047.
[13] Y. Yang, Y. Zhuang, Y. He, B. Bai, X. Wang, Fine tuning of the dimensionality of zinc silicate nanostructures and their application as highly efficient absorbents for toxic metal ions, Nano Research 3 (2010) 581–593.
[14] Y. Zhuang, Y. Yang, G. Xiang, X. Wang, Magnesium silicate hollow nanostructures as highly efficient absorbents for toxic metal ions, Journal of Physical Chemistry C 113 (2009) 10441–10445.

[15] Y. NuLi, J. Yang, J. Wang, Y. Li, Electrochemical intercalation of Mg^{2+} in magnesium manganese silicate and its application as high-energy rechargeable magnesium battery cathode, Journal of Physical Chemistry C 113 (2009) 12594–12597.

[16] N. Taghavinia, G. Lerondel, H. Makino, A. Yamamoto, T. Yao, Y. Kawazoe1, T. Goto, Nanocrystalline Zn_2SiO_4:Mn^{2+} grown in oxidized porous silicon, Nanotechnology 12 (2001) 547–551.

[17] S. Alavi, J. Dexpert-Ghys, B. Caussat, High temperature annealing of micrometric Zn_2SiO_4:Mn phosphor powders in fluidized bed, Materials Research Bulletin 43 (2008) 2751–2762.

[18] Q. Lu, J. Li, Low-temperature synthesis of Y_2SiO_5:Eu^{3+} powders using mesoporous silica and their luminescence properties, Optical Materials 33 (2011) 381–384.

[19] P. Mohanty, S. Ram, Thermodynamic lattice instability driving bulk amorphization in Eu^{3+}-doped Al_2O_3 mesoporous composites, Materials Letters 53 (2002) 287–295.

[20] R.P. Sreekanth Chakradhar, B.M. Nagabhushana, G.T. Chandrappa, K.P. Ramesh, J.L. Rao, Solution combustion derived nanocrystalline Zn_2SiO_4:Mn phosphors: a spectroscopic view, The Journal of Chemical Physics 121 (2004) 10250–10259.